The Correlation Between Black Hole Accretion and Star Formation Rate Based on IllustrisTNG100-1

Qiyu Li

School of Physics, University of Science and Technology of China, Hefei, China

liqiyu9832@mail.ustc.edu.cn

Abstract. Observational results suggest the co-evolution relationship between the supermassive black holes (SMBHs) and their host galaxies. However, the definitive conclusion of the correlation between the star formation rate (SFR) and central black hole accretion rate (BHAR) remains unclear. In this paper, the correlation between the BHAR and SFR is investigated in terms of cosmological simulation IllustrisTNG100-1. In simulation, BHs are divided into 2 types (quasar state and kinetic state) based on their accretion speed and the feedback mechanisms between the two are different. The strong positive correlation between BHAR and SFR for quasar state BHs and low-mass kinetic state BHs is revealed. However, for high mass kinetic-state BHs, the SFR manifestation a BHAR and BH mass-independent randomly distribution. According to the analysis, this phenomenon is attributed to the environmentally insensitive, self-regulate accretion rate for high mass BHs at late time. The properties of these BHs are described, which offers a guideline for high mass AGNs observation and theorical investigations on their accretion and feedback.

1. Introduction

According to observational results, supermassive black holes (SMBHs) are considered to reside in all massive galaxy center. Accreting BHs in the center of galaxies, also known as active galactic nuclei (AGN), can inject large amount of energy to their host galaxies, which is a process called AGN feedback. Observational studies have shown the correlations between the masses of SMBHs and the properties of their host galaxies. Some scholars argued that the mass of SMBHs is strongly correlated with the mass of their host bulges [1, 2]. Other study results imply the co-evolution of central BHs and stellar mass of host galaxies [3-5].

Both star formation and BHs accretion need a supply of gas, thus observational studies are expected to manifest the correlation between the two. Several studies have aimed on the link between black hole accretion rate (BHAR) and star formation rate (SFR). However, a definitive conclusion remains unknown. Many reports an increase in the average BHAR-SFR relation for high luminosity AGNs [6-8], while others find low correlation between the two [9, 10]. There are also some studies that includes low luminosity AGNs reports that the significant correlation between BHAR and SFR only exists in galaxies with high luminosity AGNs at low redshift, and there are no correlations at lower luminosities at high redshift [11, 12].

Possible reasons for these contradictory results include selection bias, sample size, difficulties of estimating SFR and BHAR through photometric measurements, and the co-dependence of SFR and BHAR on host galactic stellar mass [13]. For example, Page et al. reported a suppression correlation

between the SFR and BHAR for samples with X-ray luminosities higher than 10^{44} erg/s [14]. Harrison et al., however, found no such suppression when studying on a statistically larger sample size, proving that the negative correlation reported by Page et al. was biased owing to the small sample size [15].

Modern cosmological numerical simulations, on the other hand, provide big sample size without the difficulty estimating SFR and BHAR form observational data. Cosmological simulations have made tremendous progress over the last decade. Based on the results, it is possible to get structure similar to observational results, in terms of galaxy star formation rates, sizes and morphologies, etc. [16-19]. With modern high-resolution simulations, studies on SMBHs and host galaxy properties can test our idea of AGN feedback models and provide guideline for observational studies.

In this paper, the correlation between the SFR and BHAR will be investigated based on cosmological simulation IllustrisTNG. Since most observational studies focus on local universe, the results at redshift z=0 are mainly discussed, but higher redshift results are still provided. The rest part of the paper is organized as follows. Section 2 describes the database and corresponding methods utilized in this paper. In section 3, the correlations between SFRs and BHs properties are investigated and analyzed. Eventually, a brief summary will be given in Section 4.

2. Database & Methodology

2.1. IllustrisTNG

llustrisTNG is the successor of Illustris simulation. It runs with the adaptive mesh refinement code Arepo assuming a ΛCDM universe with cosmology parameter reported by Planck 2015 [20]: $\Omega_{\Lambda,0} = 0.6911$, $\Omega_{\mathrm{m},0} = 0.3089$, $\Omega_{\mathrm{b},0} = 0.0486$, $\sigma_8 = 0.8159$, $\mathrm{n_s} = 0.9667$ and $\mathrm{h} = 0.6774$. The IllustrisTNG project consists of three flagship runs, with three different simulation sizes: cubes of 300, 100, and 50 Mpc side length, which are identified as TNG300, TNG100, and TNG50, respectively. The TNG100 (which is used in this paper) and TNG300 simulations were presented in 5 papers almost simultaneously [21-26]. The details of galaxy formation model and black hole feedback can be found in Refs. [21, 23]. Here, only a brief overview is given. The BHs in TNG are seeded with $\mathrm{M_{BH}} = 8 \times 10^5 \mathrm{M_\odot h^{-1}}$ in all FoF halos with mass larger than $5 \times 10^{10} \mathrm{M_\odot h^{-1}}$. BHs then grow through pure Bondi accretion, with an upper limit set by the Eddington rate. The AGN feedback affects the host galaxy in two modes. The BHs in high-accretion state correspond to a quasar-like mode thermal feedback that heats the nearby gas, while the kinetic mode corresponding to the low-accretion state aims to test the idea of black hole-driven kinetic winds. The transition from the low to high accretion state feedback modes happens when:

$$\frac{\dot{M}_{\mathrm{Bondi}}}{\dot{M}_{\mathrm{Edd}}} \geq \chi, \tag{1}$$

where

$$\chi = min\left[0.02\left(\frac{M_{BH}}{10^8 M_\odot}\right)^{2,} 0.1\right] \tag{2}$$

For high-accretion mode, the liberated feedback energy is

$$\Delta\dot{E}_{high} = \epsilon_{f,high}\epsilon_r \dot{M}_{BH} c^2, \tag{3}$$

where $\dot{\mathrm{M}}_{\mathrm{BH}}$ is the estimated black hole mass accretion rate, ϵ_{r} is the radiation efficiency (is set to 0.2 in TNG), and $\epsilon_{\mathrm{f,high}} = 0.1$. For low-accretion kinetic mode, the feedback energy is parameterized as

$$\Delta\dot{E}_{low} = \epsilon_{f,kin}\dot{M}_{BH} c^2, \tag{4}$$

where

$$\epsilon_{f,kin} = min\left[\frac{\rho}{0.05\rho_{SF\ thresh}}, 0.2\right], \tag{5}$$

ρ is the gas density around the black hole particle and $\rho_{\mathrm{SF\ thresh}}$ is the density threshold for star formation.

With the exception of AGN feedback, IllustrisTNG also includes supernova (SN) feedback, which is implemented through wind particle. Unlike the original Illutris model, the direction of wind particles in TNG model is initialized randomly, making the winds isotropic. The initial velocity is

$$v_w = max\left[\kappa_w \sigma_{DM}\left(\frac{H_0}{H(z)}\right)^{1/3}, v_{w,min}\right], \tag{6}$$

where $\kappa_{\mathrm{w}} = 7.4$, σ_{DM} is the local dark matter velocity dispersion (one-dimensional) and $v_{\mathrm{w,min}} = 350\mathrm{km/s}$ the injection velocity floor. The wind velocity floor prevents wind mass loading factor from becoming unphysically large in low-mass halos, which is written as:

$$\eta_w = \frac{2}{v_w^2} e_w (1 - \tau_w), \tag{7}$$

where parameter τ_{w} is thermal energy fraction, e_{w} is metallicity dependent efficiency factor, making the mass loading factor bigger in low metallicity environments.

2.2. API and data sample

The TNG Subhalos (can be seen as galaxies) are identified using the Subfind algorithm. For this work, only the subhalo data from TNG100-1 is used. For the SFR and subhalo star mass, the sum within twice the stellar half mass radius are utilized (SubhaloSFRinRad and SubhaloMassInRadType4, respectively). According to the TNG Data specifications, the Eddington accretion rate is calculated as

$$\dot{M}_{edd} = \frac{4\pi G M_{BH} m_p}{\epsilon_r \sigma_T c}, \tag{8}$$

Here, $\epsilon_{\mathrm{r}} = 0.2$ is the radiative efficiency parameter, σ_{T} is the Thomson scattering cross section, c is light speed in vacuum and m_{p} is proton mass.

For comparison with observational studies, the BH bolometric luminosity is computed based on the BH model given by Churazov et al. [27]. For radiatively efficient BHs with Eddington ratio $\lambda_{\mathrm{Edd}} > 0.1$, the bolometric luminosity is calculated as

$$L_{bol} = \frac{\epsilon_r}{1 - \epsilon_r} \dot{M}_{BH} c^2, \tag{9}$$

For radiatively inefficient BHs with Eddington ratio $\lambda_{\mathrm{Edd}} \leq 0.1$, the bolometric luminosity is calculated as

$$L_{bol} = 0.1 L_{Edd} (10\lambda_{Edd})^2 = 10\lambda_{Edd} \epsilon_r \dot{M_{BH}} c^2 \tag{10}$$

A total of 25329 subhalos with $M_{\mathrm{BH}} > 10^6 M_{\odot}/h$ are selected at redshift z = 0. All of them are considered to have only 1 center black hole since the total amount of BHs with mass above $10^6 M_{\odot}/h$ is 25353. Therefore, the number of subhalos contain more than 1 BH is no larger 24, or 0.09%. For redshift z = 0, these numbers are 16259, 16294, 35, 0.2% and for redshift z = 4, they are 3124, 3134, 10, 0.3%, respectively. The $M_{\mathrm{star}} - M_{\mathrm{BH}}$ diagrams of our sample are shown in Figure 1.

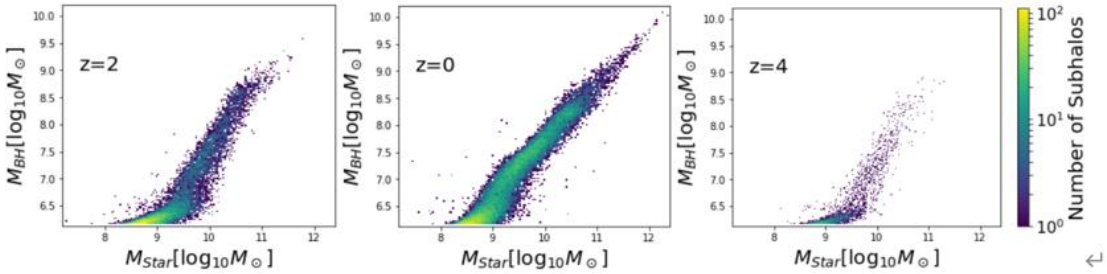

Figure 1. BH populations in BH mass versus total stellar mass of BH host subhalos diagrams in TNG100-1 at different redshift (a)z=0, (b)z=2, (c)z=4, color code by the Number of subhalos.

3. Results & Discussion

3.1. SFR versus BH Accretion Properties

The relationship between SFR and BH bolometric luminosities L_{bol} (derived from BH accretion rate, according to (8)(9)) are investigated. The results show significant positive correlation between SFR and L_{bol} with the spearman coefficient ρ= 0.592, ρ= 0.792, ρ= 0.811 at redshift z=0, z=2, z=4, respectively. The positive correlation is much stronger especially at higher redshift, as shown in Figure. 2. Red fitting lines using the ordinary least square fitting with 95% confidence region give:

$$log_{10}\left(\frac{SFR}{M_\odot/yr}\right)|_{z=0} = (-8.22 \pm 0.13) + (0.183 \pm 0.003)\, log_{10}\left(\frac{L_{bol}}{erg/s}\right) \quad (11)$$

$$log_{10}\left(\frac{SFR}{M_\odot/yr}\right)|_{z=2} = (-16.2 \pm 0.4) + (0.382 \pm 0.005)\, log_{10}\left(\frac{L_{bol}}{erg/s}\right) \quad (12)$$

$$log_{10}\left(\frac{SFR}{M_\odot/yr}\right)|_{z=4} = (-17.8 \pm 0.5) + (0.426 \pm 0.011)\, log_{10}\left(\frac{L_{bol}}{erg/s}\right) \quad (13)$$

The overall population distribution in SFR-L_{bol} diagram tends to move from top-right to bottom-left, indicating a general slower star formation and BH accretion at a lower redshift, as depicted in Figure 3. The SFR scales also with BH Eddington ratio (seen from Figure 4). The spearman coefficients at redshift z=0, z=2, z=4 are $\rho = 0.391$, $\rho = 0.668$, $\rho = 0.743$, respectively. However, this strong positive correlation is largely predictable, due to the strong correlation between Eddington ratio λ_{Edd} and bolometric luminosity L_{bol}.

Here the spearman coefficient of SFR-Eddington ratio correlation at z=0 is obviously lower than at higher redshift, and the same phenomenon can also be found in SFR-L_{bol} correlation. One of the reasons is the samples distribution tends to spread out at lower redshift. Additionally, some subhalos behave special. In z=0 and z=2 diagram, a part of massive subhalos is distinguished from the others with a clear behavior difference. They don't follow the positive correlation presented in Eqs. (11)-(13). As illustrated in Figs. 2 and 4, they clear split from the band that most of lower mass BHs lay in. These massive subhalos will be investigated in the following subsection.

3.2. Some Abnormal Massive BHs

In SFR-M_{Star} diagram and SFR - M_{BH} diagrams are exhibited in Fig. 5, where the abnormal subhalos are revealed clearly. SFR distribution “main-band” disappears when BH mass is big enough. Besides, in massive subhalos, the SFR become unpredictable and completely random other than a clear upper-limit which is same as the “main-band”.

These subhalos share some common properties. They all have central BH with M_{BH} larger than a redshift-dependent mass (for z = 0, it’s around $M_{BH} = 1.3 \times 10^8 M_\odot$ and for z=2, it’s around $M_{BH} =$

$2.5 \times 10^8 M_\odot$). Moreover, these BHs have resemble Eddington rate and bolometric luminosity. In addition, all these BHs are in low-state feedback mode(kinetic), with $\lambda_{Edd} < \chi$ (given in Eqs. (1) and (2)). It should be noted that not all BHs in low-state mode behaves like these massive BHs. On the contrary, as shown in Fig. 6, the Eddington rate and bolometric luminosity of low-mass BHs in low-state mode gradually change with BH mass. Besides, their SFR tends to converge to the high mode "main-band". The difference also exists in SFR - L_{bol} relation between low mass and high mass BHs in low-state mode. As presented in Fig. 7, for low mass low-state samples, they still have a generally strong positive SFR-L_{bol} correlation, but no such correlation is found for high mass low-state samples.

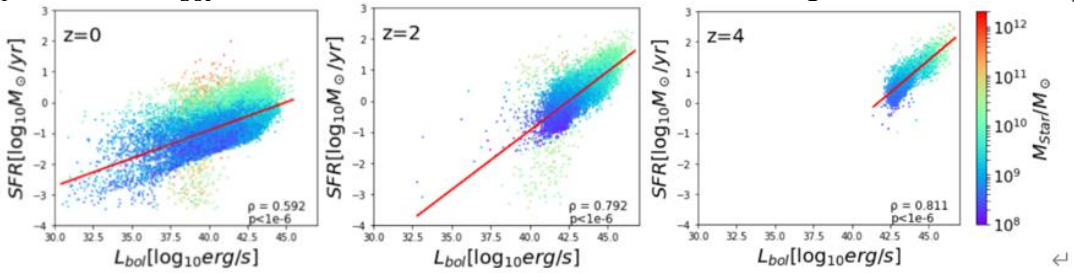

Figure 2. SFR as a function of BH bolometric luminosities (equivalently, BH accretion rate) diagrams at different redshift (a) z = 0, (b) z = 2, (c) z = 4, color code by subhalo stellar mass M_{Star} . At the bottom-right corner, the corresponding spearman coefficient ρ and corresponding p-value are given. The red line in each panel is the best fit line using least square fitting.

Figure 3. Average SFR and Average BH bolometric luminosities L_{bol} versus redshift. The red line represents average SFR, and the green line represents average BH bolometric luminosity.

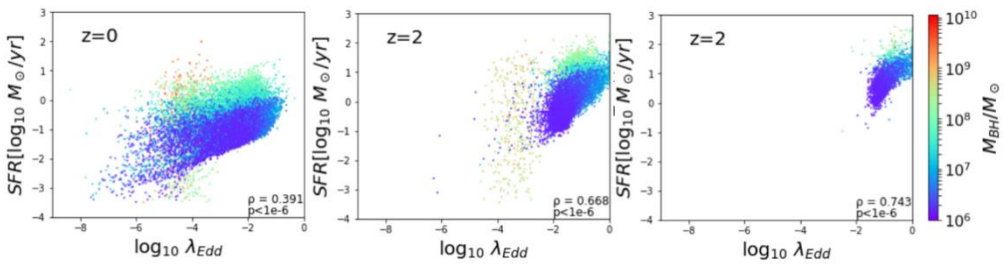

Figure 4. SFR versus Eddington ratio at redshift (a)z=0, (b)z=2, (c)z=4, color-coded by M_{BH}. At the bottom-right corner, the corresponding spearman coefficient ρ and corresponding p-value are given.

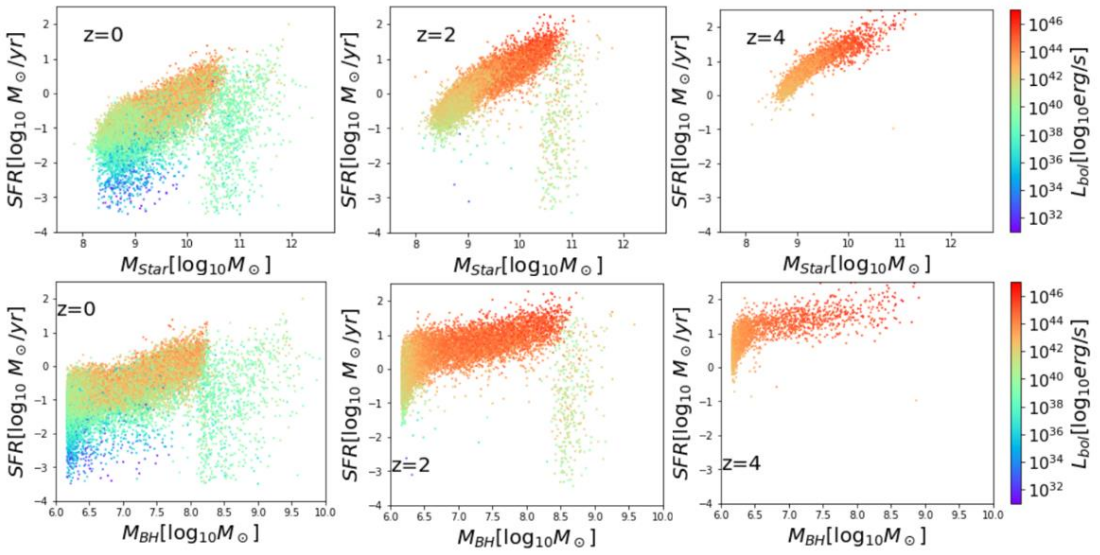

Figure 5. Top row. SFR versus subhalo stellar mass M_{Star} diagrams at different redshift (a) z = 0, (b) z = 2, (c) z = 4; 2. Bottom row: SFR versus BH mass M_{BH} diagrams at different redshift (d) z = 0, (e) z = 2, (f) z = 4, color code by BH bolometric luminosity L_{bol}.

Overall, these BHs at z=0 are all in low-state accretion mode, with Eddington ratio no larger than 10^{-4}, BH mass larger than $1.3 \times 10^{8} \mathrm{M}_{\odot}$ and the bolometric luminosity within 10^{38}~10^{42} erg/s. The possible reason for this SFR random distribution phenomenon in these subhalos is that the self-regulate accretion rate for high mass BHs at late times. With the fact that high mass BHs in high-state (quasar) are barely found in the sample, making these BH accretion not sensitive to surrounding environment. Hence, the SFR in these subhalos show no correlation with BHAR. On the other hand, in low mass case, the factor of slow BH accretion is mainly considered as the surrounding gas density, which will lead to an SFR-related BHAR.

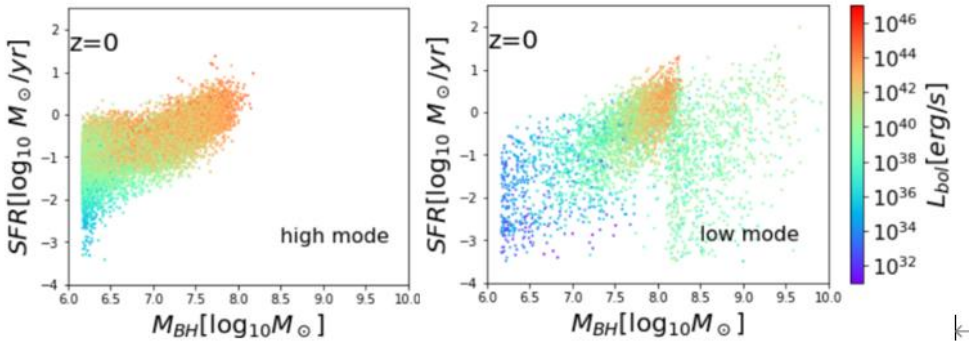

Figure 6. SFR versus BH mass M_{BH} in (a)high, (b) low feedback mode at redshift z = 0, color-coded by BH bolometric luminosity L_{bol}.

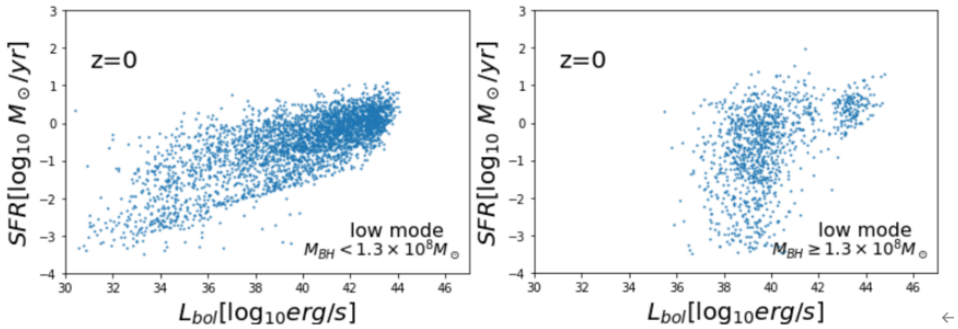

Figure 7. SFR versus BH bolometric luminosity L_{bol} diagram of BHs in low-state feedback mode(kinetic) at z=0. Left panel: BH mass $M_{\rm BH} < 1.3 \times 10^8 M_\odot$; Right panel: BH mass $M_{\rm BH} \geq 1.3 \times 10^8 M_\odot$. Here, the separation based on mass is a roughly estimation, and there is no clear threshold, so some high luminosity high mass BHs behaves like low mass BHs.

3.3. Limitation

Nevertheless, the results presented in this paper has some limitations and drawbacks. Due to the lack of the data of high mass BHs at early time in simulation, the threshold mass is only roughly estimated and provide no numerical information about the threshold mass–redshift correlation. Besides, the trigger of this self-regulate accretion and the underlying physical mechanism is unclear. The history of these high mass BHs can be tracked in future work to provide more information about their co-evolution with host galaxies. Finally, one of the most important things is that whether this self-regulate accretion exists and the way it effects host-galaxy star formation in real universe remains to be conformed in observational studies. However, the relatively low BH bolometric luminosity (around 10^{38}~10^{42} erg/s) making it hard to detect and be distinguished from other source radiations.

4. Conclusion

In summary, this paper investigates the SFR–BHAR correlation based on TNG100-1 at different redshift with 25353 samples for z=0, 16259 for z=2 and 3124 for z=0. All data used are within twice the stellar mass radius assuming only one central BH in a subhalo. As for the results, to be specific, they show strong positive correlation between SFR and BHAR for quasar-state BHs and low mass kinetic-state BHs. However, for high mass kinetic-state BHs, the SFR manifestation a BHAR and BH mass-independent randomly distribution. According to the analysis, this phenomenon is due to the environmentally insensitive, self-regulate accretion rate for high mass BHs at late time. Nevertheless, the underlying physical mechanism and whether this phenomenon exists in real universe is unclear. In the future, the history of these self-regulate BHs can be tracked in TNG and in other cosmological simulations to further investigate the underline physics. Overall, these results offer a guideline for high mass SMBHs observation and theorical studies on their accretion.

References

[1] Magorrian, John, et al. The Demography of Massive Dark Objects in Galaxy Centers. The Astronomical Journal 115 (1998): 2285-305.
[2] Gebhardt, Karl, et al. A Relationship between Nuclear Black Hole Mass and Galaxy Velocity Dispersion. The Astrophysical Journal 539 (2000): L13-L16.
[3] Alexander, D. M., and R. C. Hickox. What Drives the Growth of Black Holes? New Astronomy Reviews 56 (2012): 93-121.
[4] Richstone, D., et al. Supermassive Black Holes and the Evolution of Galaxies. Nature 385 (1998): A14.
[5] Heckman, Timothy M., and Philip N. Best. The Coevolution of Galaxies and Supermassive Black Holes: Insights from Surveys of the Contemporary Universe. Annual Review of

Astronomy and Astrophysics 52 (2014): 589-660.
[6] Harris, Kathryn, et al. Star Formation Rates in Luminous Quasars at 2 < Z < 3. Monthly Notices of the Royal Astronomical Society 457 (2016): 4179-94.
[7] Chen, Chien-Ting J., et al. A Correlation between Star Formation Rate and Average Black Hole Accretion in Star-Forming Galaxies. The Astrophysical Journal 773 (2013): 3.
[8] Zhuang, Ming-Yang, and Luis C. Ho. The Interplay between Star Formation and Black Hole Accretion in Nearby Active Galaxies. The Astrophysical Journal 896 (2020): 108.
[9] Shimizu, T. Taro, et al. Herschel Far-Infrared Photometry of the Swift Burst Alert Telescope Active Galactic Nuclei Sample of the Local Universe - Iii. Global Star-Forming Properties and the Lack of a Connection to Nuclear Activity. Monthly Notices of the Royal Astronomical Society 466 (2017): 3161-83.
[10] Azadi, Mojegan, et al. Primus: The Relationship between Star Formation and Agn Accretion. The Astrophysical Journal 806 (2015): 187.
[11] Santini, P., et al. Enhanced Star Formation Rates in Agn Hosts with Respect to Inactive Galaxies from Pep-Herschel Observations. Astronomy and Astrophysics 540 (2012): A109.
[12] Lutz, D., et al. The Laboca Survey of the Extended Chandra Deep Field South: Two Modes of Star Formation in Active Galactic Nucleus Hosts? The Astrophysical Journal 712 (2010): 1287-301.
[13] Harrison, C. M. Impact of Supermassive Black Hole Growth on Star Formation. Nature Astronomy 1 (2017): 0165. Print.
[14] Page, M. J., et al. The Suppression of Star Formation by Powerful Active Galactic Nuclei. Nature 485 (2012): 213-16.
[15] Harrison, C. M., et al. No Clear Submillimeter Signature of Suppressed Star Formation among X-Ray Luminous Active Galactic Nuclei. The Astrophysical Journal 760 (2012): L15.
[16] Dubois, Yohan, Marta Volonteri, and Joseph Silk. Black Hole Evolution - Iii. Statistical Properties of Mass Growth and Spin Evolution Using Large-Scale Hydrodynamical Cosmological Simulations. Monthly Notices of the Royal Astronomical Society 440 (2014): 1590-606.
[17] Vogelsberger, M., et al. Properties of Galaxies Reproduced by a Hydrodynamic Simulation. Nature 509 (2014): 177-82.
[18] Pillepich, Annalisa, et al. First Results from the Illustristng Simulations: The Stellar Mass Content of Groups and Clusters of Galaxies. Monthly Notices of the Royal Astronomical Society 475 (2018): 648-75.
[19] Davé, Romeel, et al. Simba: Cosmological Simulations with Black Hole Growth and Feedback. Monthly Notices of the Royal Astronomical Society 486 (2019): 2827-49.
[20] Collaboration, Planck, et al. Planck 2015 Results. A&A 594 (2016): A13.
[21] Pillepich, Annalisa, et al. Simulating Galaxy Formation with the Illustristng Model. Monthly Notices of the Royal Astronomical Society 473 (2018): 4077-106.
[22] Nelson, Dylan, et al. First Results from the Illustristng Simulations: The Galaxy Colour Bimodality. Monthly Notices of the Royal Astronomical Society 475 (2018): 624-47.
[23] Weinberger, Rainer, et al. Supermassive Black Holes and Their Feedback Effects in the Illustristng Simulation. Monthly Notices of the Royal Astronomical Society 479 (2018): 4056-72.
[24] Springel, Volker, et al. First Results from the Illustristng Simulations: Matter and Galaxy Clustering. Monthly Notices of the Royal Astronomical Society 475 (2018): 676-98.
[25] Marinacci, Federico, et al. First Results from the Illustristng Simulations: Radio Haloes and Magnetic Fields." Monthly Notices of the Royal Astronomical Society 480 (2018): 5113-39. Print.
[26] Naiman, Jill P., et al. First Results from the Illustristng Simulations: A Tale of Two Elements - Chemical Evolution of Magnesium and Europium. Monthly Notices of the Royal Astronomical Society 477 (2018): 1206-24.
[27] Churazov, E., et al. Supermassive Black Holes in Elliptical Galaxies: Switching from Very Bright to Very Dim. Monthly Notices of the Royal Astronomical Society 363 (2005): L91-L95.